INTERNATIONAL JOURNAL FOR NUMERICAL AND ANALYTICAL METHODS IN GEOMECHANICS
Int. J. Numer. Anal. Meth. Geomech., **22**, 515–548 (1998)

ANALYSIS OF A FULL SCALE *IN SITU* TEST SIMULATING REPOSITORY CONDITIONS

A. GENS[1]*, A. J. GARCIA-MOLINA[1], S. OLIVELLA[1], E. E. ALONSO[1] AND F. HUERTAS[2]

[1] *E.T.S de Ingenieros de Caminos, Technical University of Catalunya, 08034 Barcelona, Spain*
[2] *ENRESA, Emilio Vargas 7, 28043 Madrid, Spain*

SUMMARY

Coupled thermo-hydro-mechanical (THM) analyses have been used to examine the interacting phenomena associated with the simultaneous heating and hydration of an engineered bentonite barrier placed in a drift excavated in granite. The specific problem studied is an *in situ* test being carried out in the underground laboratory at Grimsel (Switzerland). After describing the test and the theoretical formulation, the results of a coupled THM analysis using the best parameter estimation currently available are presented and discussed. The effect of various features of analysis are explored by means of additional analyses in which each of those features are varied, one at the time. Finally, sensitivity analyses have been carried out to examine some critical aspects of the *in situ* test design. Performance of coupled THM analyses has led to a better understanding of the various inter-related phenomena occurring during heating and hydration of the engineered clay barrier. © 1998 John Wiley & Sons, Ltd.

Key words: coupled analysis; expansive clay; granite, radioactive waste; thermo-hydro-mechanical analysis; unsaturated soils

1. INTRODUCTION

Engineered barriers constitute a basic element in the conceptual design of repositories for radioactive waste in deep geological media. Compacted expansive clay is often the material of choice for constructing barriers in repositories located in natural clays or crystalline rocks. The evaluation of the safety of the envisaged disposal schemes requires a good understanding of the performance of the barrier and the host medium in the near-field zone. However, barrier behaviour is highly complex, involving coupled thermo-hydro-mechanical phenomena that take place during heating and hydration of the clay barrier. Numerical analysis can be an effective way to bridge the gap between the theoretical and empirical understanding of the individual processes occurring and the resulting overall performance of the barrier. Consequently, formulations for coupled thermo-hydro-mechanical finite element analysis involving unsaturated geomaterials are receiving increasing attention.[1–3]

A general parametric analysis of the global engineered barrier behaviour is not viable because of the number of different variables affecting the results. However, the performance of full-scale tests under conditions similar to those likely to be encountered in practice provide a very useful

* Correspondence to: A. Gens, ETS Ingenieros de Caminos, C. yP. Technical University of Catalunya, 08034 Barcelona, Spain

CCC 0363–9061/98/070515–34$17.50

Received 30 March 1995
Revised 26 September 1997

framework in which to consider the analysis of engineered barriers. Data obtained during the tests will also provide the basic information for model validation. Naturally, the time-scale required to study the long-term behaviour cannot be reproduced, so analysis must concentrate on the phenomena occurring in the early transient phase. Success in providing a good representation of the physical processes occurring at this stage will nevertheless increase confidence in the ability of the model to provide reasonable predictions in the longer term.

In this context, ENRESA (the Spanish agency for the management and storage of radioactive waste) is carrying out a full-scale heating test (FEBEX) of an engineered barrier made up of compacted bentonite blocks. The test is performed in the underground laboratory of the Grimsel test site (Switzerland) excavated in granite. Analysis plays a central role in the planning, performance and interpretation of a test of this kind. In the definition of the FEBEX work programme, it is envisaged that numerical analysis will be used as an aid for planning and design, as a prediction tool, and as a basic instrument for the interpretation of field results during and after the performance of the test.

In this paper, selected analysis of the series of numerical computations carried out for the preliminary design and planning of the full-scale test are presented. Special attention will be given to the fully coupled thermo-hydro-mechanical analysis as they are very useful as an aid to understanding the variety of interacting phenomena likely to occur during the test. The effect of several critical features of the analysis are reviewed. The results of some sensitivity analysis concerning basic test variables are also discussed.

2. DESCRIPTION OF THE FEBEX *IN SITU* HEATING TEST

The design of the FEBEX test is closely related to the present Spanish reference disposal concept that contemplates a mined-type repository excavated at depth consisting of an array of horizontal full-faced drilled drifts of 2·4 m diameter. Along the axis of the gallery a number of 0·90 m diameter canisters 4·54 m long would be placed. The thermal load of each canister is envisaged to be 1200 W. Each canister would be surrounded by a buffer made up of compacted bentonite blocks that fill the space between successive canisters and between canisters and the host medium.

The FEBEX test consists in placing two heaters having the same dimensions as the canisters of the reference disposal concept in the centre of a recently excavated drift at the Grimsel test site. A Tunnel Boring Machine has been used for excavation in order to minimize the disturbed zone around the tunnel. The diameter of the gallery is 2·27 m, very close to the reference value. The free space between heaters and granite will be backfilled with blocks of compacted clay made up of La Serrata bentonite quarried in Southeastern Spain. The main characteristics of the bentonite are as follows: fraction of particles smaller than 2 μm = 93 per cent, specific surface 33 m^2/g, liquid limit, $w_l = 103$ and plasticity index, $w_p = 49$. The mineralogical analysis of the particles smaller than 2 μm indicates that 93 per cent of the clay fraction is smectite.

The host rock in the area where the experiment is located is granite belonging to the Central Arae formation. It is a very sound rock with a small number of discontinuities, often associated with the presence of lamprophyre dykes. Further information on the test site geology is given in Reference 4. The rock is initially saturated with a regional flow pattern modified by the presence of the tunnels excavated for the Grimsel Test Site. The water pressures in the area of the experiment measured before tunnel excavation are in the range of 0·5–0·7 MPa. The envisaged total length of the experiment is 13 m and it is isolated from the rest of the gallery by a concrete bulkhead. A schematic view of the test layout is shown in Figure 1.

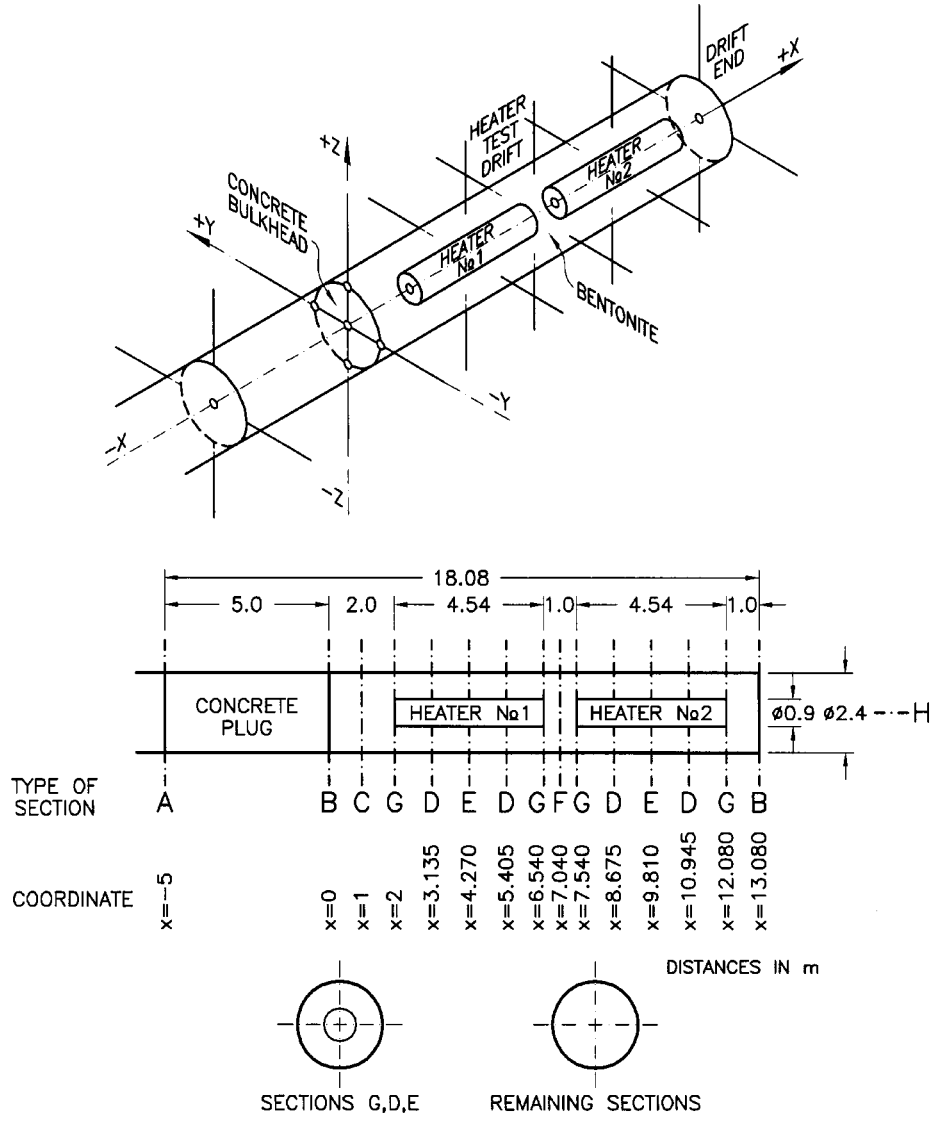

Figure 1. FEBEX test lay out and instrumented sections

The tests will be fully instrumented both in the bentonite and in the granite. Figure 1 also shows the main instrumented sections. It is planned that the heaters will initially supply a constant heat flow until the bentonite reaches the maximum allowable temperature of 100°C. Afterwards the heater power will be controlled in order to keep this maximum temperature constant. It is envisaged that heating will be applied during a continuous 3-year period. Afterwards, the power will be switched off and a 6 month cooling period will follow before dismantling.

The main processes expected to occur during the test will be the heating of the buffer and surrounding host medium and the hydration of the buffer by water drawn from the nearby granite. Both heating and hydration influence the mechanical behaviour and response. Consequently, the test involves an interaction of thermal, hydraulic and mechanical phenomena. The simulation of those phenomena is the main goal of the coupled analysis reported herein. A number of simplifying assumptions have been made. For instance, an average mass permeability of the granite is used to describe the hydraulic property of the rock, localized water entries through discontinuities are not explicitly considered. Similarly, an homogeneous buffer is assumed disregarding the joints between the bentonite blocks and the potential gap between rock and buffer. Those features are introduced in the second phase of 2-D analyses, but they are out of the scope of this paper.

3. THEORETICAL FRAMEWORK

Modelling the problem outlined above requires the performance of coupled thermo-hydro-mechanical (THM) analysis that is formulated using a multi-phase, multi-species approach. In the following, variables may include a subscript and a superscript. The subscript refers to the phase (s for solid, l for liquid and g for gas), whereas the superscript indicates the species (w for water and a for dry air). The liquid phase may contain water and dissolved air and the gas phase may be a mixture of dry air and water vapour. Air is considered as a single species. Given the mineral types present in the problem analysed, solution/precipitation of solids is not considered.

A basic step in the development of a theoretical approach to the problem is the selection of the physical phenomena to be included in the modelling. In this case the following ones have been considered:

Heat transport:

(1) Heat conduction (Fourier's law).
(2) Heat advection (by liquid water and vapour)

Water flow:

(1) Darcy flow,
(2) Vapour diffusion,
(3) Phase changes.

Mechanical behaviour:

(1) Thermal expansion of bentonite and granite,
(2) Swelling of the bentonite depending on suction and stress,
(3) Elastic deformation of the granite.

Local equilibrium is assumed throughout. The theoretical framework is composed of three main parts that are summarized below: balance equations, equilibrium restrictions and constitutive equations. A more general and detailed description of this formulation is presented elsewhere.[1]

3.1. Balance equations

The balance equations are established for the porous medium as a whole. The compositional approach[5] is adopted to establish the mass balance equations. It consists of balancing the species rather than the phases. The following balance equations are considered:

Balance of energy:

$$\frac{\partial}{\partial t}(E_s\rho_s(1-\phi)+E_l\rho_l S_l\phi+E_g\rho_g S_g\phi)+\nabla\cdot(\mathbf{i}_c+\mathbf{j}_{E_s}+\mathbf{j}_{E_l}+\mathbf{j}_{E_g})=f^E \tag{1}$$

where E_s, E_l and E_g are specific internal energies corresponding to each phase, ρ_s, ρ_l and ρ_g are the densities of the three phases, ϕ is porosity, S_l is the volumetric liquid fraction and S_g is the volumetric gas fraction with respect to pore volume. Naturally, $S_l+S_g=1$. $\mathbf{i}_c$ is the non-advective (conduction) heat flux and $\mathbf{j}_{E_s}$, $\mathbf{j}_{E_l}$, $\mathbf{j}_{E_g}$ are the advective energy flux of each of the three phases with respect to a fixed reference system. The most relevant advection energy fluxes correspond to vapour and liquid water motion. f^E is the energy supply per unit volume of medium.

Balance of mass of water:

$$\frac{\partial}{\partial t}(\theta_l^w S_l\phi+\theta_g^w S_g\phi)+\nabla\cdot(\mathbf{j}_l^w+\mathbf{j}_g^w)=f^w \tag{2}$$

where θ_l^w and θ_g^w are the mass of water per unit volume of liquid and gas, respectively. $\mathbf{j}_l^w$ and $\mathbf{j}_g^w$ denote the total mass flux of water in the liquid and gas phases with respect to a fixed reference system and f^w is the external mass supply of water per unit volume of medium.

Balance of mass of air:

$$\frac{\partial}{\partial t}(\theta_l^a S_l\phi+\theta_g^a S_g\phi)+\nabla\cdot(\mathbf{j}_l^a+\mathbf{j}_g^a)=f^a \tag{3}$$

where θ_l^a and θ_g^a are the mass of dry air per unit volume of liquid and gas, respectively. $\mathbf{j}_l^a$ and $\mathbf{j}_g^a$ indicate the total mass flux of water in the liquid and gas phases with respect to a fixed reference system. f^a is the external mass supply of air per unit volume. Without loss of generality, this equation may be dropped if a constant pressure is assumed for the gas phase.

Balance of momentum (equilibrium):

$$\nabla\cdot\boldsymbol{\sigma}+\mathbf{b}=\mathbf{0} \tag{4}$$

where $\boldsymbol{\sigma}$ are stresses and $\mathbf{b}$ body forces.

3.2. Equilibrium restrictions

Thanks to the compositional approach adopted, phase changes do not appear explicitly in the formulation. The assumption of local equilibrium implies that the species concentration in the various phases can be considered as dependent variables. Equilibrium restrictions are given for the concentration of water vapour in gas and of dissolved air in water.

The mass of water vapour per unit volume of gas (θ_g^w) is determined via the psychrometric law:[6,7]

$$\theta_g^w=(\theta_g^w)^0\exp\left(\frac{-(P_g-P_l)M_w}{R(273{\cdot}15+T)\rho_l}\right) \tag{5}$$

where P_l and P_g are liquid and gas pressures, respectively, $(\theta_g^w)^0$ is the vapour density in the gaseous phase in contact with a planar surface (i.e. when $P_g - P_l = 0$), M_w is the molecular mass of water (0·018 kg/mol), R is the gas constant (8·314 J/mol K) and T is the temperature (in degrees Celsius). $(\theta_g^w)^0$ is strongly dependent on temperature. Vapour partial pressure is computed by means of the ideal gas law.

The solubility of air in water is controlled by Henry's law:

$$\omega_l^a = \frac{P_a}{H}\frac{M_a}{M_w} \tag{6}$$

where ω_l^a is the mass fraction of air in liquid, P_a is the partial pressure of air, M_a is the molecular mass of air (0·02895 kg/mol) and $H = 10000$ MPa is Henry's constant. Note that, according to the definition of partial density, $\theta_l^a = \omega_l^a \rho_l$.

3.3. Constitutive equations

3.3.1. Thermal. It is assumed that the conductive heat flow is governed by Fourier's law:

$$\mathbf{i}_c = -\lambda \nabla T \tag{7}$$

where λ is the global thermal conductivity. The dependence of λ on degree of saturation and porosity is given by the geometric mean approximation:[8]

$$\lambda = \lambda_s^{(1-\phi)}\lambda_l^{\phi S_l}\lambda_g^{\phi(1-S_l)} = \lambda_{sat}^{S_l}\lambda_{dry}^{1-S_l} \tag{8}$$

where λ_s, λ_l and λ_g are the thermal conductivities of the individual phases, and $\lambda_{sat}(=\lambda_s^{1-\phi}\lambda_l^{\phi})$ and $\lambda_{dry}(=\lambda_s^{1-\phi}\lambda_g^{\phi})$ are the thermal conductivities for saturated and dry conditions, respectively.

The internal energies per unit mass for each phase can be written as

$$E_l = E_l^w \omega_l^w + E_l^a \omega_l^a \tag{9a}$$

$$E_g = E_g^w \omega_g^w + E_g^a \omega_g^a \tag{9b}$$

where $E_l^w = 4180{\cdot}0\,T$ (J/kg), $E_l^a = 1006{\cdot}0\,T$ (J/kg), $E_g^w = 2{\cdot}5 \times 10^6 + 1900{\cdot}0\,T$ (J/kg) and $E_g^a = 1006{\cdot}0\,T$ (J/kg). The value of E_s depends on the type of solid material.

3.3.2. Hydraulic. Liquid and gas flow follow Darcy's law:

$$\mathbf{q}_l = -\mathbf{K}_l(\nabla P_l - \rho_l \mathbf{g}) \tag{10a}$$

$$\mathbf{q}_g = -\mathbf{K}_g(\nabla P_g - \rho_g \mathbf{g}) \tag{10b}$$

where $\mathbf{K}_\alpha = \mathbf{k}\,k_{r\alpha}/\mu_\alpha$ is the permeability tensor. The intrinsic permeability tensor ($\mathbf{k}$) depends on the pore structure of the porous medium. $k_{r\alpha}$ is the value of relative permeability that controls the variation of permeability in the unsaturated regime and μ_α denotes the dynamic viscosity. In these expressions, α may stand for either l or g depending on whether liquid or gas flow is considered. $\mathbf{g}$ is the gravity vector. The variation of intrinsic permeability with porosity is given by

$$\mathbf{k} = \mathbf{k}_0 \frac{\phi^3}{(1-\phi)^2}\frac{(1-\phi_0)^2}{\phi_0^3} \tag{11}$$

where ϕ_0 is a reference porosity. The relative permeabilities of the liquid and gaseous phases are made dependent on degree of saturation according to[9]

$$S_e = \frac{S_l - S_{lr}}{S_{ls} - S_{lr}} \tag{12a}$$

$$k_{rl} = S_e^{1/2}(1 - (1 - S_e^{1/\beta})^{\beta})^2 \quad S_e \leqslant 1 \tag{12b}$$

$$k_{rg} = 1 - k_{rl} \tag{12c}$$

where S_{lr}, S_{ls} and β are material parameters.

It is also necessary to define the retention curve of the materials relating degree of saturation with suction $(P_g - P_l)$. The expression selected is[9]

$$S_e = \left(1 + \left(\frac{P_g - P_l}{P_0}\right)^{1/(1-\beta)}\right)^{-\beta} \quad P_g - P_l \geqslant 0 \tag{13}$$

where P_0 is a material parameter.

Finally, the molecular diffusion of vapour in air is governed by Fick's law:

$$\mathbf{i}_g^w = -\mathbf{D}_g^w \nabla \omega_g^w = -(\phi \rho_g S_g \tau \mathbf{D}_m^w \mathbf{I} + \rho_g \mathbf{D}_g') \nabla \omega_g^w \tag{14}$$

where $\mathbf{i}_g^w$ is the non-advective mass flux of water in gas, $\mathbf{D}_g^w$ is the dispersion tensor, ω_g^w is the mass fraction of water in gas, τ is the tortuosity and $\mathbf{D}_g'$ the mechanical dispersion tensor. In this work a constant dispersion coefficient corresponding to the molecular diffusion of vapour in air is assumed.[10]

$$D_m^w(\mathrm{m}^2/\mathrm{s}) = 5{\cdot}9 \times 10^{-12} \frac{(273{\cdot}15 + T)^{2{\cdot}3}}{P_g} \tag{15}$$

P_g is in MPa units. $\mathbf{D}_g'$ can be safely neglected if no significant air flow takes place.

3.3.3. Mechanical. In saturated porous materials, mechanical behaviour is best understood in terms of effective stress $\boldsymbol{\sigma}' = \boldsymbol{\sigma} - P_l \mathbf{m}$ where $\mathbf{m}^T$ is the auxiliary vector $[1, 1, 1, 0, 0, 0]$. For unsaturated materials it is necessary to consider two independent stress variables. Here net stresses $(\boldsymbol{\sigma} - P_a \mathbf{m})$ and capillary suction, $s = (P_g - P_l)$ have been adopted. Net stress is the excess of total stress over air pressure. If full saturation is achieved, net stress becomes effective stress.

The mechanical constitutive equation takes the incremental form

$$\mathrm{d}\boldsymbol{\sigma} = \mathbf{D}\,\mathrm{d}\boldsymbol{\varepsilon} + \mathbf{h}\,\mathrm{d}s \tag{16}$$

where $\boldsymbol{\sigma}$ is now used for net stresses, $\boldsymbol{\varepsilon}$ is the strain tensor, $\mathbf{D}$ is the constitutive stiffness matrix and $\mathbf{h}$ is a constitutive vector relating changes of suction to changes in net stresses.

For the bentonite buffer the constitutive equation used in this work is a non-linear elastic one in which the dependence of volume changes on applied stresses and suction is modelled using the state surface approach.[11,12] The following expression for volumetric strain, ε_v, is adopted:

$$\varepsilon_v = \mathbf{m}^T \boldsymbol{\varepsilon} = a \ln p + b \ln s + c \ln p \ln s \tag{17}$$

where p is the mean net stress and a, b and c are parameters. By differentiation, this equation allows the computation of K (elastic bulk modulus) and $\mathbf{h}$. A constant G (elastic shear modulus) completes the non-linear elastic model. As a first approximation it is assumed that suction changes cause volumetric strains only. Elasto-plastic laws for unsaturated materials have been

developed[13,14] that allow incorporation of temperature effects,[15] but they have not been used in this analysis.

The relationship between the basic variables, displacements, $\mathbf{u}$, at the strains $\boldsymbol{\varepsilon}$, that appear in the mechanical constitutive law is through the usual expression:

$$\boldsymbol{\varepsilon} = \tfrac{1}{2}(\nabla\mathbf{u} + \nabla\mathbf{u}^{\mathrm{T}}) \tag{18}$$

4. FEATURES OF THE ANALYSES AND MATERIAL PARAMETERS

4.1. Discretization

The numerical analysis has been carried using the finite element code CODE-BRIGHT that allows the performance of coupled thermo-hydro-mechanical analysis in 1, 2 and 3 dimensions.[16] The code was initially developed for problems involving saline media but it can be easily adapted to the analysis of other geological materials. It is able to take into account all the physical phenomena and constitutive laws discussed in the previous section.

The analyses reported in this paper take advantage of the basic axial symmetry of the problem and of the relatively long size of the heaters in order to adopt a radial one-dimensional discretization. 2-D analyses have also been performed but are not included herein. As it is believed that the gas phase will not be confined during the test, a constant gas pressure equal to atmospheric is prescribed throughout. Vapour diffusion phenomena are considered however.

Figure 2 shows the various zones present in the discretization. The main ones are zone F (bentonite buffer) and zone G (rock). The thickness of the backfill is 0·66 m and the outer boundary of the domain has been located 70 m away from the drift axis. Zones A to E attempt to reproduce as exactly as possible the preliminary design of the heater although it has little influence on the results obtained from the analysis. A liner (zone E), placed to facilitate installation, surrounds the heater and is in contact with the bentonite.

A number of results will be presented for three representative zones of the buffer: the region close to the heater, the region in the centre of the buffer and the region close to the rock. Figure 2 shows the locations of the particular nodes and elements selected for this purpose.

4.2. Material parameters

A significant number of the parameters required by the formulation described are physical constants, the values of which have been indicated in Section 3. However, there are material—specific parameters that are discussed in this section. The specific parameters used for the basic THM analysis described in Section 5 are collected in Table I. In the analyses discussed in later sections some of the parameters may be varied to check on the sensitivity of results. The alternative parameter values will be given in the appropriate section.

There is a significant amount of data concerning the materials involved in the problem obtained from laboratory and *in situ* tests. Generally, parameters for the bentonite have been determined in laboratory tests.[17]) Granite properties are mainly derived from the extensive NAGRA data-base on the rock of the Grimsel test site.[4–18] Parameters for steel and air are obtained from the literature and, in general, do not affect results significantly.

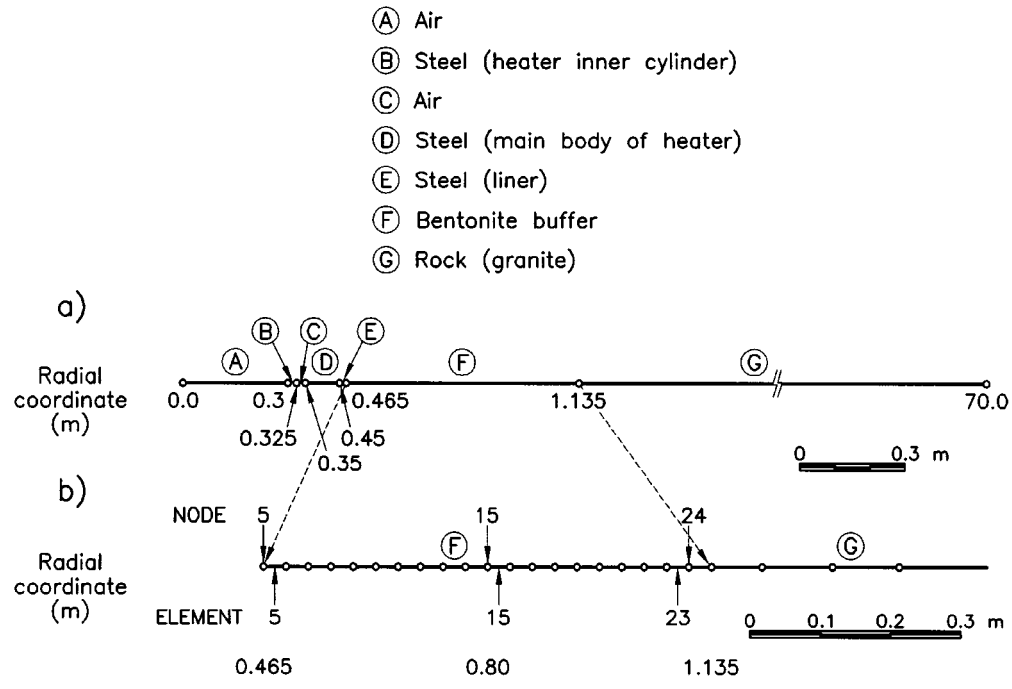

Figure 2. Discretization of the problem. Nodes and elements used in the presentation of the results are indicated

The following comments can be made regarding parameter selection:

(1) A basic parameter for temperature evolution and distribution is the thermal conductivity λ. The geometric mean law adopted for the bentonite [equation (8)] can be compared with the results of laboratory tests in bentonite[17] (Figure 3). It can be noted that the agreement is good, although the value of λ is slightly overestimated at high degree of saturation. However, in the range of interest of the test the approximation is quite close. The value of λ for the granite is based on tests performed by Nagra[18] and is taken as constant given the very low porosity of the material.

(2) The parameters for hydraulic conductivity and retention curve have been derived from laboratory permeability and suction plate tests.[17] The adopted retention curve is plotted in Figure 4(a). The effective water permeability of the bentonite is made dependent on porosity and degree of saturation according to the expression $\mathbf{K}_l = \mathbf{k} k_{rl}/\mu_l$. k_{rl} is given by equation (12b).

(3) The permeability of the granite has been determined from the backcalculation of the results of a ventilation test carried out in a drift in Grimsel.[18] In order to obtain a better agreement with the results of the field test, a different law for the variation of relative permeability with degree of saturation is incorporated in the analysis ($k_{rl} = S_l^3$). The granite retention curve used in the analysis is plotted in Figure 4(a). It is based on the retention curve shown in Figure 4(b) that has been determined in the laboratory.[19] It is surprising, nevertheless, that, according to the experimental results, the air entry value of the granite is

Table I. Material parameters for THM analysis

	Bentonite	Granite	Steel	Air
Thermal				
λ_{sat} (W/m °C)[a]	1·507	3·6	50·16	0·0026
λ_{dry} (W/m °C)[a]	0·42	3·6	50·16	0·0026
E_s/T (J/kg °C)	1091	793	460	
Hydraulic				
k_0 (m^2)[a]	2×10^{-20}[b]	10^{-18}[c]		
β	0·5	0·33		
P_0 (MPa)	50	0·1		
Mechanical				
α (°C^{-1})	10^{-5}	$7{\cdot}80 \times 10^{-6}$	$1{\cdot}20 \times 10^{-5}$	
G (MPa)	10	$1{\cdot}35 \times 10^{4}$	$8{\cdot}75 \times 10^{4}$	
K (MPa)	–[d]	$2{\cdot}92 \times 10^{4}$	$1{\cdot}17 \times 10^{5}$	
h	–[d]			

[a] For initial porosity values
[b] It corresponds to an hydraulic conductivity of 2×10^{-13} m/s at 20°C.
[c] Taken as constant, independent of porosity. It corresponds to an hydraulic conductivity of 10^{-11} m/s at 20°C.
[d] From state surface: $\varepsilon_v = -0{\cdot}12 \ln p - 0{\cdot}06 \ln s - 0{\cdot}006 \ln p \ln s$[19]

much lower than that of the bentonite. As a consequence of the adoption of this water retention curve, an extreme desaturation of the granite in the close vicinity of the buffer will be obtained in the analysis. No change of granite permeability with porosity is considered.

(4) The mechanical behaviour of the bentonite is characterized by a state surface, the parameters of which have been based on test data obtained from suction-controlled oedometer tests.[10] For the rock, a linear elastic model is used. The elastic constants are derived from the available Grimsel data base.[4]

(5) The measured value of the coefficient of thermal expansion, α, of the granite has been used in the analysis.[4] In contrast, the coefficient of thermal expansion has not been measured in the bentonite and an educated guess value of 10^{-5}°C^{-1} has been adopted.

4.3. Initial and boundary conditions

The present test design envisages that the heating elements are placed on the outside of the inner cylinder (zone B). In the analysis, therefore, a heat source is placed on the boundary between zone B and C, at a radial coordinate of 0·325 m. The boundary condition is applied as follows: first a constant heat flux is prescribed (450 W/m) until the temperature of the bentonite reaches 100°C. Afterwards, the heat flux is controlled in such a way that a constant temperature of 100°C is maintained at the liner/bentonite contact ($r = 0{\cdot}465$ m).

To set the initial conditions of the analysis of the heating *in situ* test, a preliminary stage is performed that simulates successively:

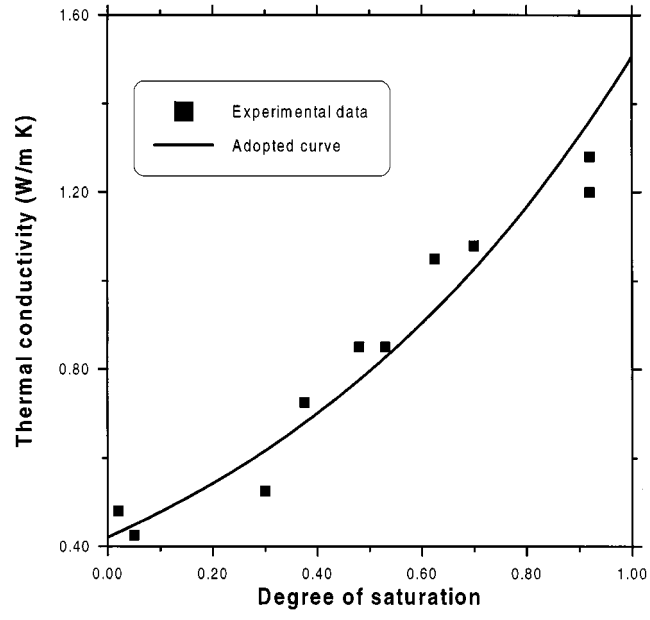

Figure 3. Variation of thermal conductivity with degree of saturation. Adopted curve and laboratory data

(1) Excavation of the drift.
(2) Establishment of equilibrium hydraulic conditions.
(3) Construction of the engineered barrier.

For this preliminary stage, an isotropic stress of 28 MPa (an average of the measured *in situ* stresses at Grimsel test side)[4] and a water pressure of 0·5 MPa have been assumed.

For the main phase of the analysis corresponding to the simulation of the *in situ* heating test, the following initial conditions are adopted:

Bentonite

(1) Porosity, $\phi = 0{\cdot}4064$,
(2) Degree of saturation, $S_l = 0{\cdot}46$,
(3) Suction, $s = 97{\cdot}3$ MPa,
(4) Initial stress, $\sigma_1 = \sigma_2 = \sigma_3 = 0{\cdot}5$ MPa.

Granite

(1) Porosity, $\phi = 0{\cdot}01$,
(2) Degree of saturation, $S_l = 1{\cdot}0$.

A constant initial temperature of 12°C is assumed throughout the analysis domain.

The initial conditions for the bentonite are based on those envisaged in the preliminary design of the test. The selected granite porosity corresponds to an average of measured values[18] and it is further assumed that desaturation of the granite due to the opening of the tunnel is negligible.

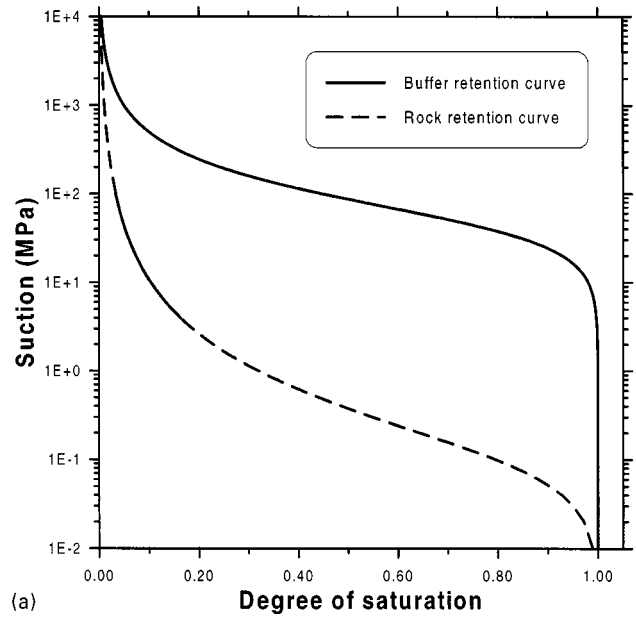

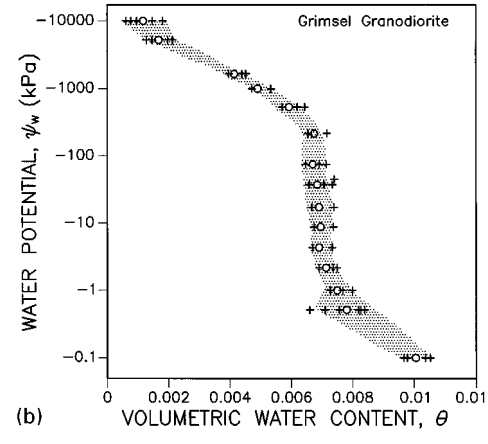

Figure 4. (a) Retention curves for compacted bentonite and granite used in the analysis; (b) Granite retention curve determined experimentally in the laboratory[18]

The outer boundary of the discretization is considered to be sufficiently far away not to be affected by the *in situ* test. Therefore, at $r = 70$ m radial stresses are set to a constant 28 MPa value, water pressure to 0·5 MPa and temperature to 12°C. Steel has a high stiffness and has been assigned an extremely low permeabiity so that the liner acts as an impervious rigid boundary subjected only to a certain amount of expansion due to heating.

5. RESULTS OF THE THERMO-HYDRO-MECHANICAL ANALYSIS OF THE *IN SITU* TEST

5.1. General

The simultaneous heating and hydration of the engineered barrier gives rise to a series of phenomena that interact with each other in a complex way. These individual phenomena must be captured adequately by the numerical analysis so that their coupled effects can be properly examined in the results of the analysis. They are now briefly reviewed.

At the inner boundary of the buffer, the main external loading is the heat flux given out by the heater. It results in both a temperature increase and, via water evaporation, a drying of the clay. Therefore, it would be expected that the degree of saturation and water pressure will decrease significantly in this region. Drying will also cause a volume reduction of the buffer material leading, in absence of other effects, to a stress reduction. An independent effect associated with the temperature increase in this zone is the expansion of the heater itself. The resulting outward displacement will cause some compression of the buffer material against the surrounding rock. Vapour arising from the drying of the inner part of the barrier will diffuse outwards until finding a cooler region where vapour will condensate causing a local increase in degree of saturation. Vapour diffusion may be therefore a significant mechanism of moisture and heat transfer.

Moving to the outer boundary, the controlling condition is the higher water pressure of the granite with respect to the bentonite suction implying a flow of water from the surrounding rock into the buffer. This hydration process will cause an increase of degree of saturation, swelling of the buffer material and a consequent increase of radial stresses in the barrier. Depending on the hydraulic characteristics of the granite, the drawing of water into the buffer may lead to desaturation of the surrounding rock with its associate reduction of permeability. The consequence may be the formation of an unsaturated barrier to water that slows down sharply the hydration process.

An additional coupling between the thermal and hydraulic aspects of the problem is provided by the variation of thermal conductivity with moisture content. As the simultaneous drying/wetting of different regions of the barrier takes place, the distribution of thermal conductivities changes and so the temperature distribution is also modified.

In this section, the results of the basic THM analysis of the *in situ* test using the material parameters and boundary conditions indicated in Section 4 are presented and discussed. In spite of the strongly coupled nature of the problem, thermal, hydraulic and mechanical results are reviewed separately noting their mutual interactions where required.

5.2. Thermal results

The variation of temperature with time for three selected points of the buffer during the 3-year heating stage is shown in Figure 5. There is a rapid increase of temperature corresponding to the constant heat flux phase (450 W/m). After the temperature in the liner/bentonite contact reaches 100°C, subsequent temperature increases in the buffer are small. The 100°C maximum bentonite temperature is achieved after 21 days heating. The heat flux required to keep this temperature constant during the three years of test duration is shown in Figure 6. It can be observed that the significant reduction in the heating power required after reaching the maximum temperature is followed by a very gentle increase in the second part of the test. This increase reflects the higher thermal conductivity of the buffer material due to the progress of saturation. After 3 years, the

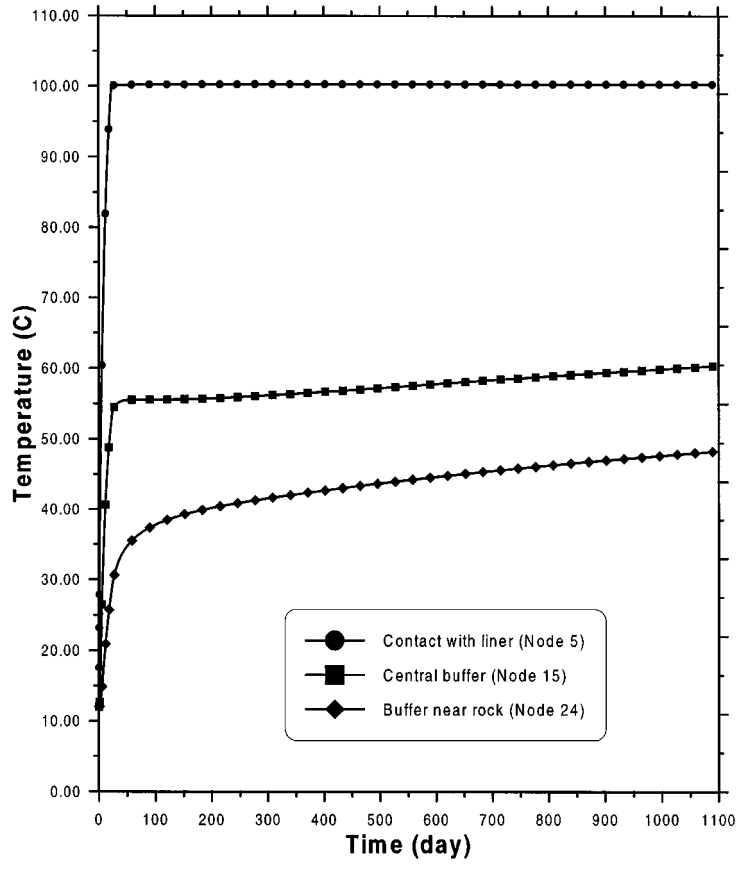

Figure 5. Variation of temperature with time. Heating phase. THM analysis

heating phase is followed by a cooling stage in which the heaters are switched off. The variation of temperature with time during this stage is plotted in Figure 7. It can be noted that a fast rate of cooling occurs leading to a high uniformity of temperature across the buffer. The distributions of temperature for various times in the barrier and immediately surrounding rock are shown in Figure 8(a) whereas Figure 8(b) contains the same distributions only for the rock. It is apparent that after 3-years heating the temperature field has extended to about a distance of 30 m, temperature increases beyond this point are less than 1°C.

5.3. Hydraulic aspects

The variations of the degree of saturation for three representative points in the buffer are shown in Figure 9. Their behaviour is very different from each other. The buffer point in contact with the liner undergoes a severe drying, the degree of saturation drops below 0·15 and remains practically constant afterwards. No hydration occurs in this zone throughout the test. In contrast, the buffer material near the rock experiences a monotonic increase in degree of saturation due to hydration

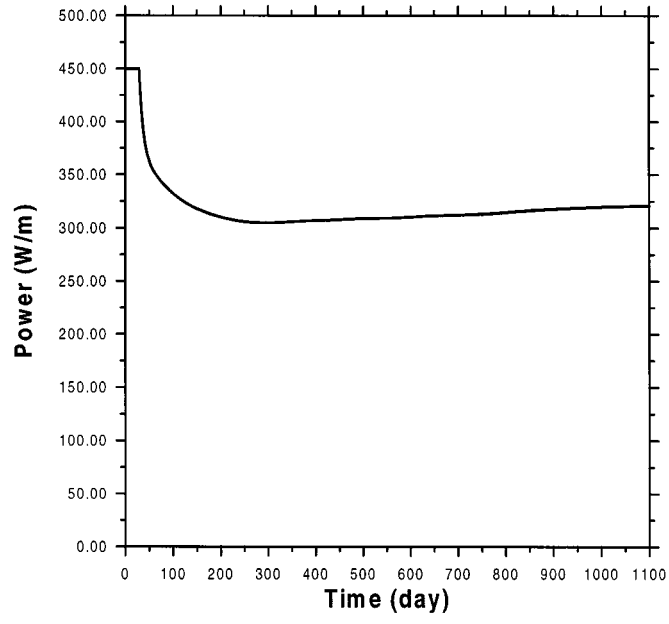

Figure 6. Variation of power from the heater with time. Heating phase. THM analysis

from the surrounding granite. However, at the end of the heating stage full saturation has not been achieved. The behaviour of the central part of the buffer is very enlightening. There is an initial increase in saturation due to the condensation of the vapour coming from the inner buffer regions. However, some drying takes place eventually due to the combined effect of temperature increase and reduced vapour arrival. Finally, a limited amount of hydration is observed by effect of water coming from the outer barrier regions.

The distributions of degree of saturation for various times (including the end of the cooling stage) in the near region are presented in Figure 10(a). The isochrone for a time of 21 days shows clearly the effects of evaporation/condensation in the inner part of the buffer. Afterwards, distributions reflect the slow progressive hydration of the barrier. The degree of saturation rises somewhat in the area near the heater during the cooling phase. Also very noticeable, is the high desaturation occurring in the granite, a direct consequence of the retention curve adopted in the analysis. The distributions of water pressure [Figure 10(b)] show the same trends but, naturally, a smooth transition is observed now across the bentonite/granite boundary.

5.4. Mechanical aspects

Changes in water pressures and stresses occurring during the test result in the succession of porosity distributions plotted in Figure 11. The outer zones of the barrier swell (due to wetting) whereas the inner regions contract (due to drying and heater expansion effect). In fact, the overall change of porosity is controlled by the relative movement of granite (practically zero) and heater (due to thermal expansion). The distribution of radial displacements [Figure 12(a)] demonstrates this clearly. Stresses have to readjust to keep, at all times, the total volume change prescribed by

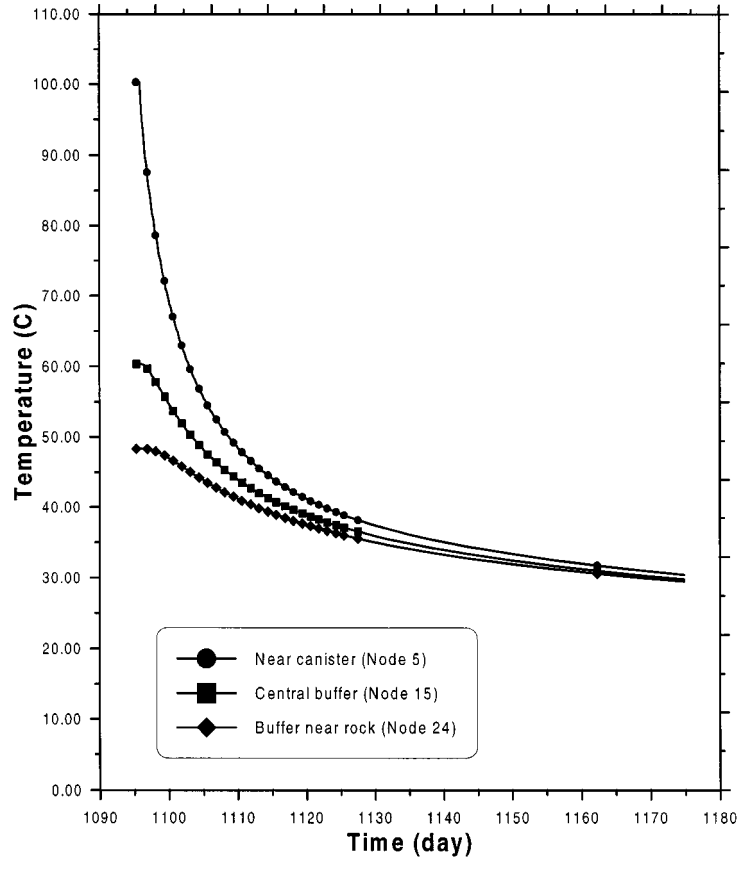

Figure 7. Variation of temperature with time. Cooling phase. THM analysis

the conditions at the interfaces. The computed radial stress distributions are shown in Figure 12(b). The increase in radial stress is monotonic and reaches values of the order of 0·3–0·4 MPa. A proportion of this increase is due to the expansion of the heater. If the analysis is run without heater thermal expansion, radial stress increment is reduced to 0·2–0·3 MPa. The sensitivity of the radial stress increment and its distribution across the barrier to the constitutive law type and parameters has not been fully explored. Therefore, the results of this analysis concerning mechanical variables should be treated as indicative only and should be checked using more advanced elasto-plastic models.[13–15]

The distributions of displacements in the granite are presented in Figure 13(a). Movement magnitudes are small and mainly due to temperature increase. Radial stress increases [Figure 13(b)] are relatively large, of the order of 3–5 MPa and, again, are mainly caused by the effects of temperature increase. The stress applied by bentonite swelling to the rock is only about 0·3–0·4 MPa, about an order of magnitude smaller.

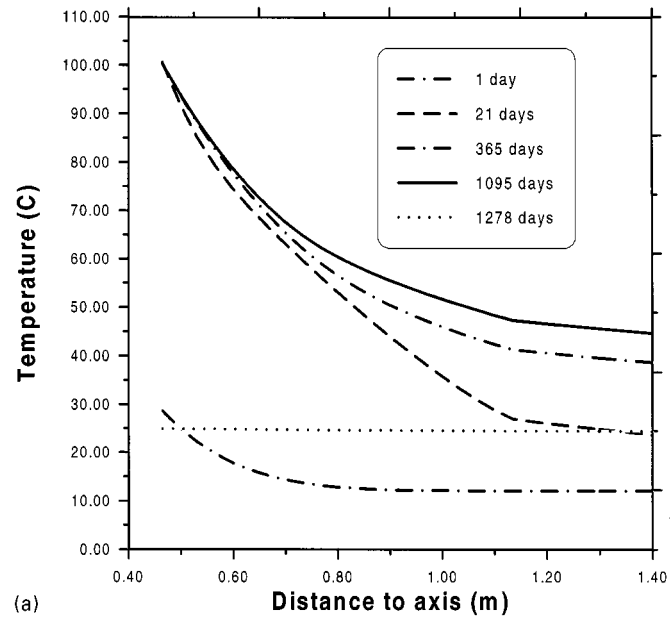

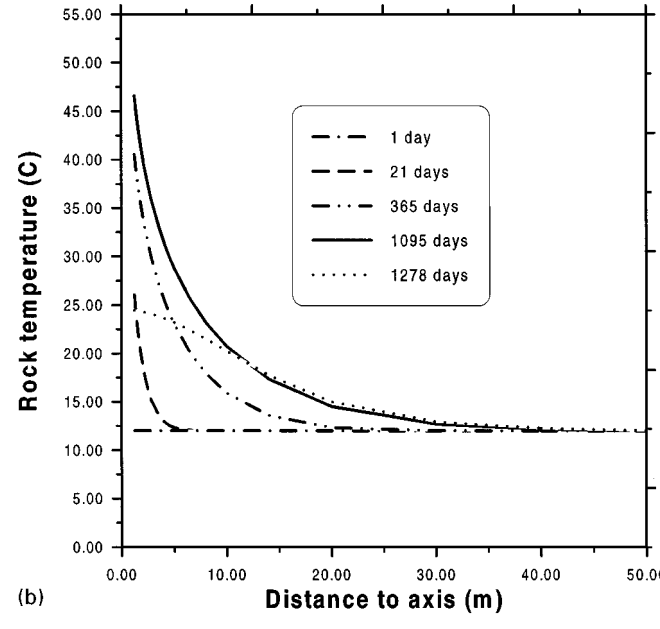

Figure 8. (a) Distribution of temperatures at various times. Near region. THM analysis; (b) Distribution of rock temperature at various times. THM analysis

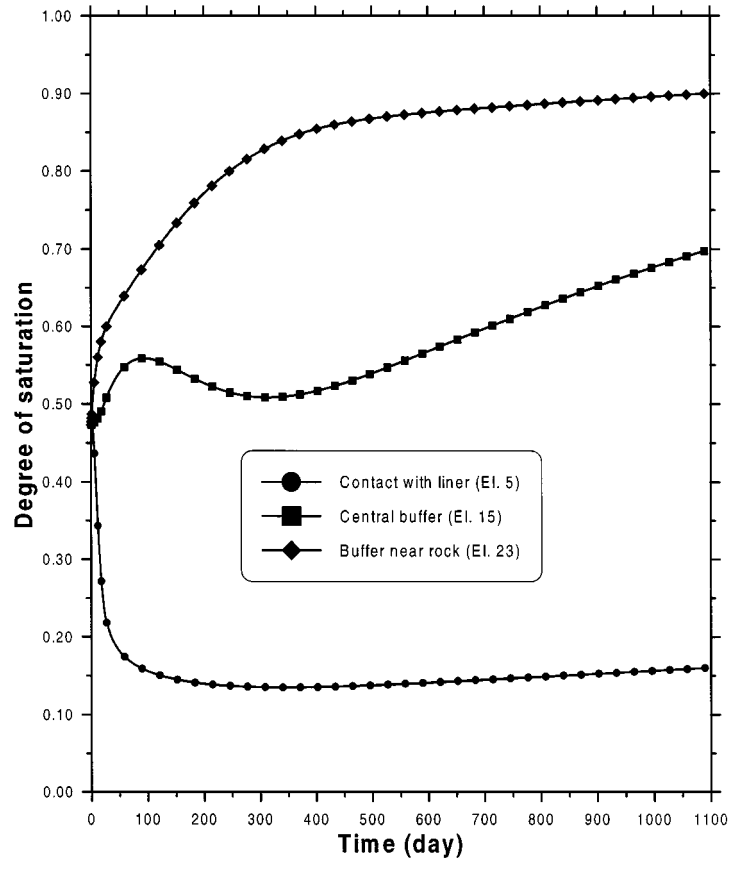

Figure 9. Variation of the degree of saturation with time. Heating phase. THM analysis

6. ANALYSES USING ALTERNATIVE HYPOTHESIS

Examination of the results of a simple analysis is useful to observe the interplay of the various phenomena involved but it is unable to isolate the effect of critical factors on the problem. In this section the influence of three of those factors (considered either illustrative or uncertain) will be reviewed using the results of three analyses performed using alternative hypothesis. The factors examined are:

(1) Vapour diffusion,
(2) Retention curve of the granite,
(3) Absence of thermal loading.

The results of these additional analyses are compared with those obtained in the basic case described in the previous section. Only variables demonstrating relevant differences between analyses are shown and the heating phase alone has been simulated.

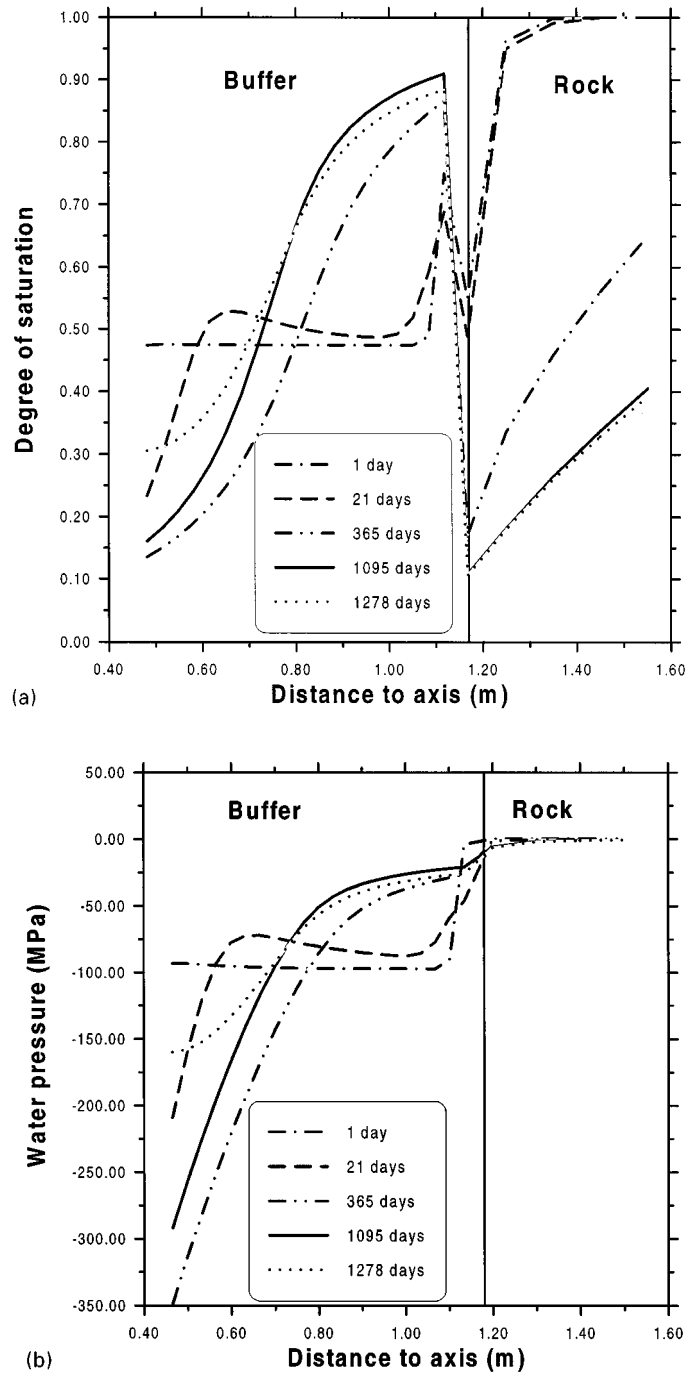

Figure 10. (a) Distribution of degree of saturation at various times. Near region. THM analysis; (b) Distribution of water pressures at various times. Near region. THM analysis

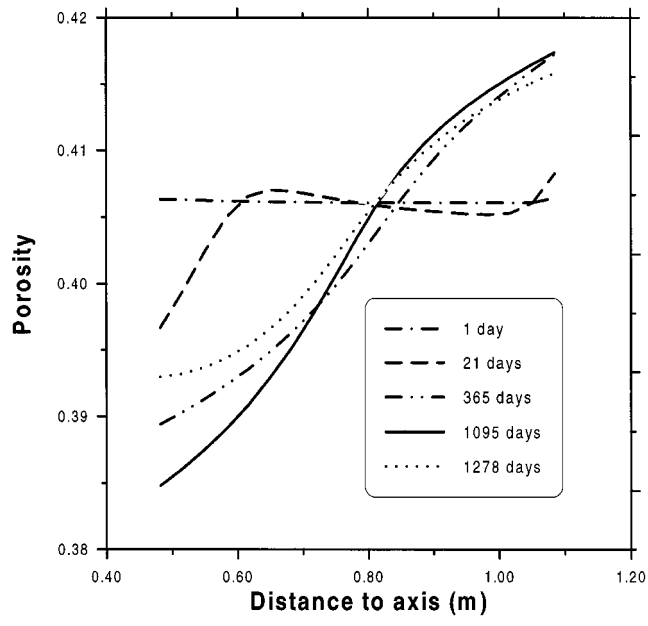

Figure 11. Distribution of buffer porosity at various times. THM analysis

6.1. Vapour diffusion

An important feature of the analysis is the consideration of heat and moisture transport through vapour diffusion. As described in Section 5, evaporation and condensation of vapour have significant effects on the evolution of water content and water pressure throughout the buffer. To demonstrate the effect of the vapour presence more directly, an analysis has been performed in which the coefficient of vapour diffusion has been set to zero. Therefore, no mass nor energy transport takes place in the gaseous phase. The rest of parameters and boundary conditions are left unchanged.

The evolution of the degree of saturation for three different points of the buffer are compared in Figure 14. It can be observed that at a point close to the canister the degree of saturation remains practically constant if vapour diffusion is not considered. Air quickly becomes vapour-saturated preventing further evaporation. This is in strong contrast with the results of the basic THM analysis where vapour diffusion is allowed. The early variation of the intermediate point in the THM analysis can be seen to be due to condensation/evaporation phenomena. The degree of saturation increase of the latter part of this evolution is similar in the two analyses and is due to hydration of the buffer from the host rock.

The buffer closer to the granite reaches a smaller degree of saturation if no vapour diffusion is considered because there is no significant transfer of moisture from the hot to the cooler zones of the buffer. The differences in hydration rates naturally result also in differences in water pressure, porosity changes and radial stress increases (e.g. Figure 15). The need to consider the vapour diffusion terms in the formulation is, therefore, clearly demonstrated.

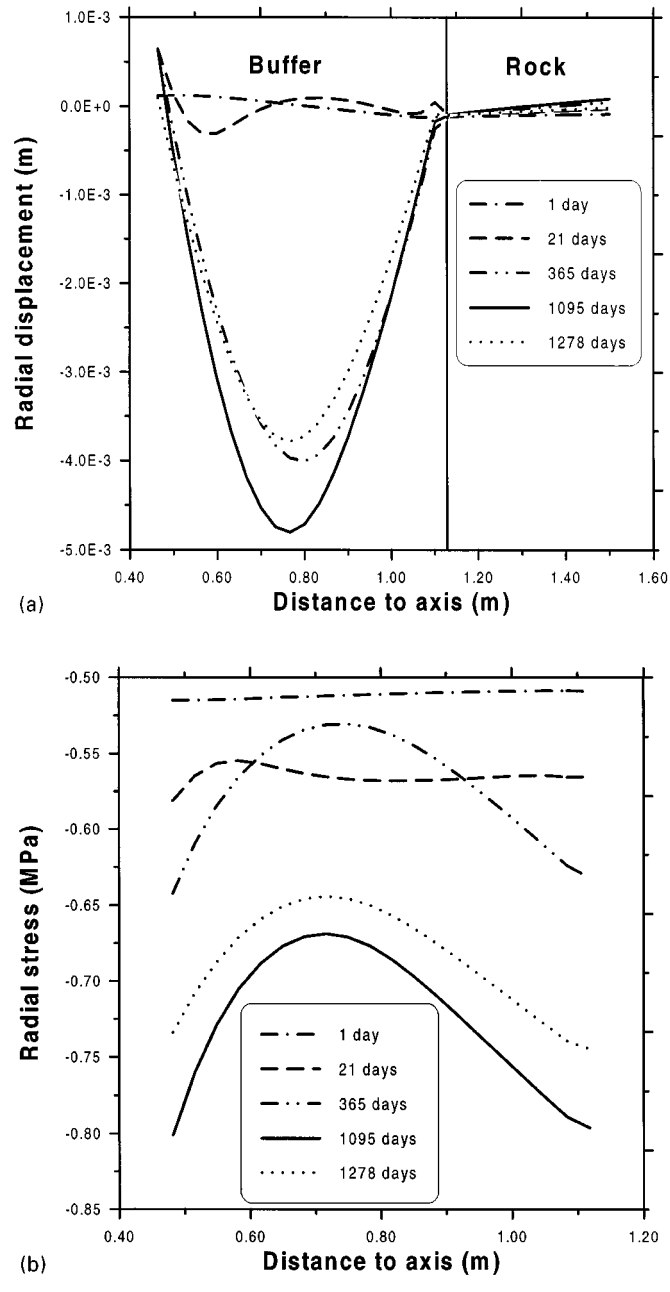

Figure 12. (a) Buffer radial displacement distributions at various times. THM analysis. Positive values indicate outward displacements; (b) Buffer radial stress distributions at various times. THM analysis

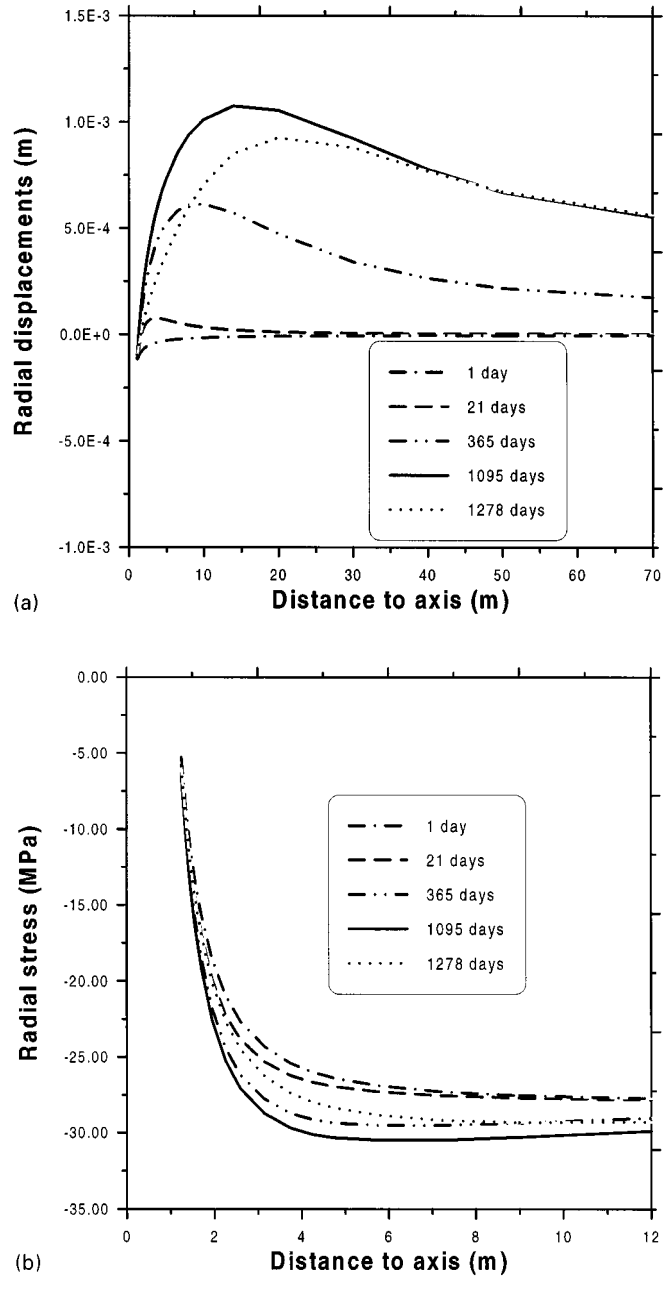

Figure 13. (a) Rock radial displacement distributions at various times. THM analysis. Positive values indicate outward displacements; (b) Rock radial stress distributions at various times. THM analysis

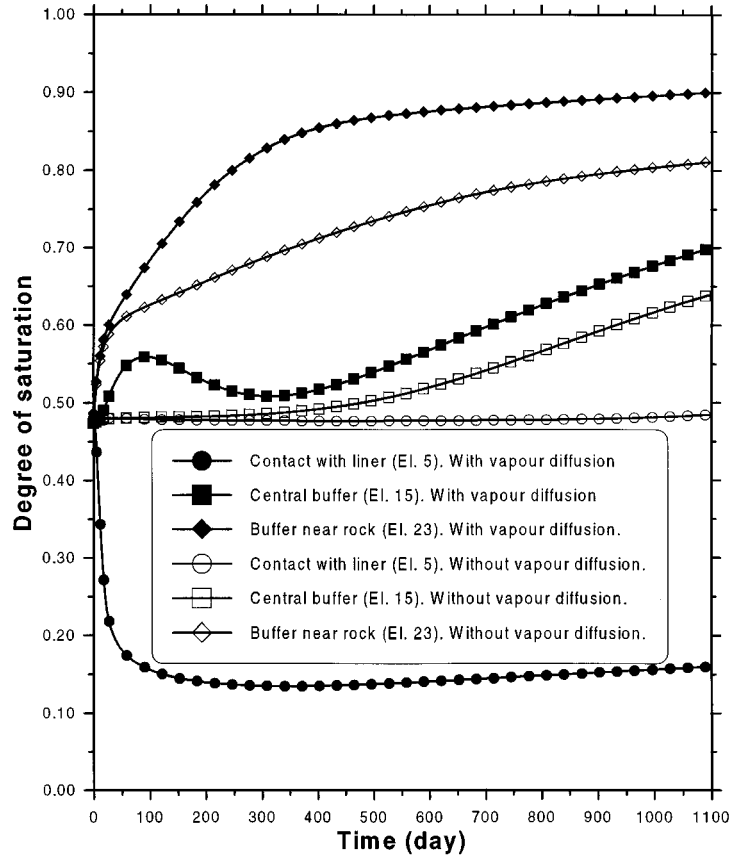

Figure 14. Comparison of the variation of the degree of saturation with time. Analysis with and without vapour diffusion

6.2. Retention curve of the granite

As indicated earlier, laboratory tests results showing a low desaturation threshold have been used to derive the retention curve of the granite used in the analysis. This fact leads to a very significant desaturation of the granite in the region close to the buffer that controls many of the aspects of behaviour of the *in situ* test. The field measurements obtained during the ventilation test performed in Grimsel[18] suggest, however, that the air entry value of the rock may in fact be higher. To examine directly the effect of this potential desaturation, an analysis has been performed using a retention curve for the granite with a much higher air entry value (Figure 16).

As Figure 17(a) demonstrates, the effects of using this alternative retention curve are dramatic. Nearly complete hydration takes place during the 3-years of the heating phase. The figure also shows that the granite remains basically saturated throughout. Large differences are also observed in Figure 17(b) in which the evolution of degree of saturation is plotted. From the beginning a much faster increase in moisture content can be observed at the point close to the rock. In the other two points considered, the early variation is similar in the two analyses shown

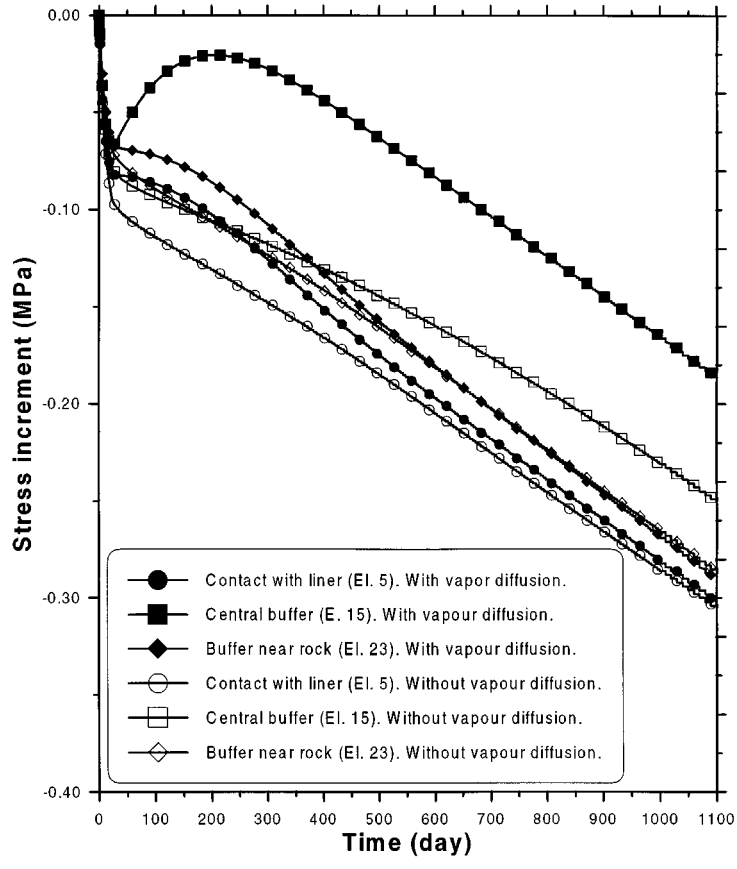

Figure 15. Comparison of the radial stress increment for analysis with and without vapour diffusion

but, soon, significant hydration occurs leading to a practically fully saturated state at the end of the heating stage. The variations and distributions of temperature, porosity and stresses are naturally also affected by the faster hydration process. As Figure 18 shows, the temperature in the buffer is now higher than in the basic THM analysis reflecting the larger thermal conductivity of the saturated material.

6.3. Absence of thermal loading

To isolate the effects due to temperature increase, a coupled isothermal hydromechanical analysis (HM) has been performed. The results are compared with the reference thermo-hydro-mechanical analysis (THM). It can be observed (Figure 19) that for the points in the vicinity of the rock and in the central part of the buffer, hydration proceeds much more slowly. At the point close to the liner no moisture content changes are computed since neither hydration nor drying by heating takes place. Overall buffer saturation at the end of the three years is lower in the HM analysis due to two main reasons:

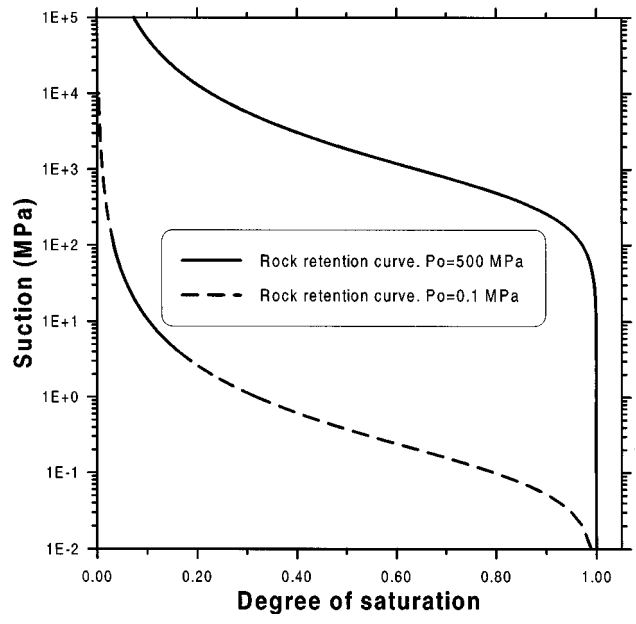

Figure 16. Retention curves for the granite used in the analyses with and without rock desaturation

(1) Lack of moisture transfer by evaporation/condensation, so that the permeability in the rock/buffer interface remains lower than in the THM analysis.
(2) Effective water permeability is smaller at lower temperatures.

Because of the limited hydration that takes place swelling pressure developed in the buffer is modest. Since thermal heater expansion is also absent the resulting increment of radial stresses is quite small (Figure 20).

7. SENSITIVITY ANALYSES

A number of features of the *in situ* test, such as, required heating power and hydration times, require special consideration as they are directly related to basic test design and expected test performance. Parametric studies have been carried out covering the range of possible values of some critical variables.

7.1. Heating power

The *in situ* test specification states that a temperature of 100°C should be reached in the bentonite at a reasonable time so that a significant part of the heating phase is performed under a condition of constant temperature in the liner/bentonite contact. A sensitivity study of the time required to reach 100°C has been carried out varying the heating power value. The results shown in Figure 21 demonstrate that the relationship between time required to reach 100°C and heating power is very non-linear. The time required decreases very quickly at higher values of heating power whereas the temperature of 100°C is not reached if the power falls below 300 W/m

approximately. Naturally, those times are a lower bound of the real times as no lateral heat dissipation is accounted for in 1-D analysis.

Once a temperature of 100°C is reached, the power applied to the heater is varied in order to maintain a constant temperature in the bentonite close to the central cylinder. As Figure 22 shows, the heating power required at this stage is strongly dependent on the thermal conductivity of the buffer. Higher thermal conductivities require a longer initial stage to reach the required temperature and, afterwards, its rate of power reduction is more gentle. The opposite occurs for low thermal conductivity values. The heating power obtained in the reference THM analysis (Figure 6) fits well in the results of Figure 22. Initially, it follows the curve corresponding to the initial value of thermal conductivity ($\lambda = 0{\cdot}756$ W/m K). However, as hydration progresses thermal conductivity increases and the results of the THM analysis move towards the curves that correspond to higher λ values. It is confirmed, therefore, that the increase in heating power required during the later stages of the heating phase is the direct consequence of a higher overall thermal conductivity resulting from moisture content increase.

7.2. Hydration times

A basic unknown in the future performance of the *in situ* test is the time required for hydration. Obviously, it will depend on the values of the permeability of the buffer material and host rock. Given the importance of this factor, a sensitivity analysis has been performed in which the bentonite permeability has been held constant while the granite permeability has been varied over three orders of magnitude.

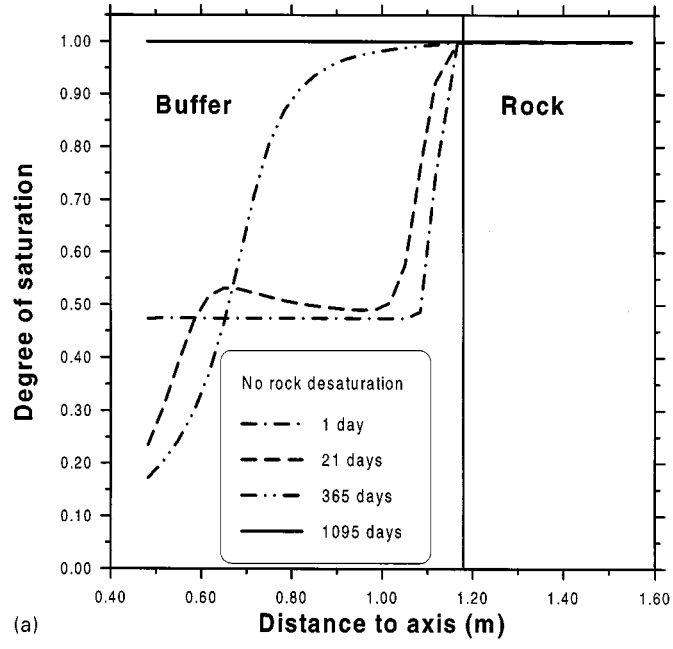

Figure 17. (a) Distributions of degree of saturation at various times. Near region. Analysis with no rock desaturation; (b) Comparison of the variations of the degree of saturation with time. Analyses with and without rock desaturation

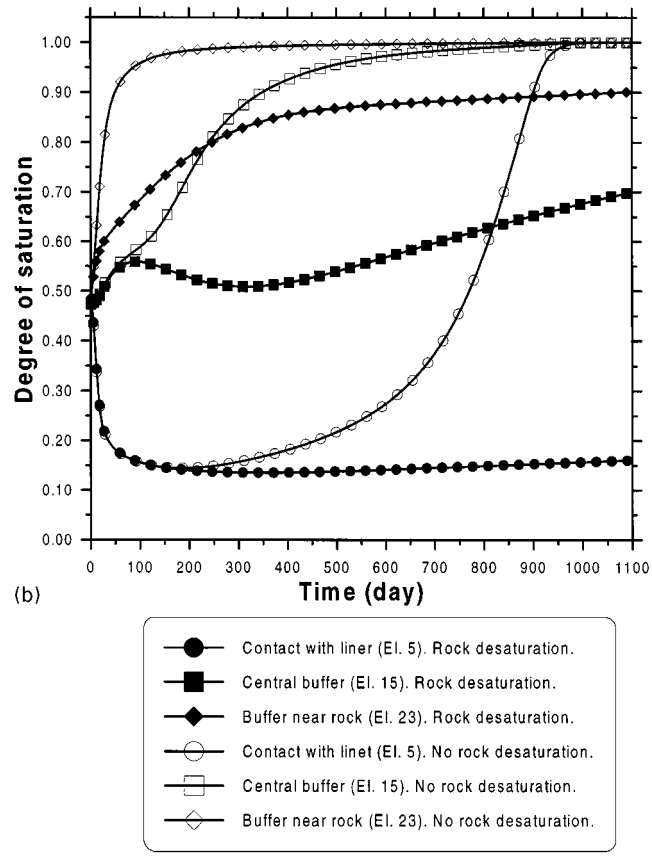

Figure 17. Continued

As hydration is an asymptotic process, in order to remove ambiguities, the hydration time is arbitrarily taken as that required for a point located at 15 cm from the central heater edge to reach a value of zero suction. It corresponds, therefore, to a significant buffer hydration rather than to its full saturation. It should be expected that if the rock permeability is high compared to that of the buffer, the permeability of the bentonite will control hydration times. In contrast, the amount of water released by the rock and, therefore, the rate of hydration will be controlled by the granite permeability if its value is sufficient low.

The results shown in Figure 23 demonstrate clearly that this distinction between two different hydraulic behaviour regions is correct. The results are plotted in non-dimensional form for greater generality. It is apparent that if the ratio between the saturated permeability of the granite with respect to that of the bentonite is higher than approximately 300, hydration times are controlled by the bentonite permeability value, whereas the opposite occurs for lower values of the same ratio. It should be pointed out that this curve is only valid for the hydraulic boundary conditions and the specific laws of variation of permeability with suction and

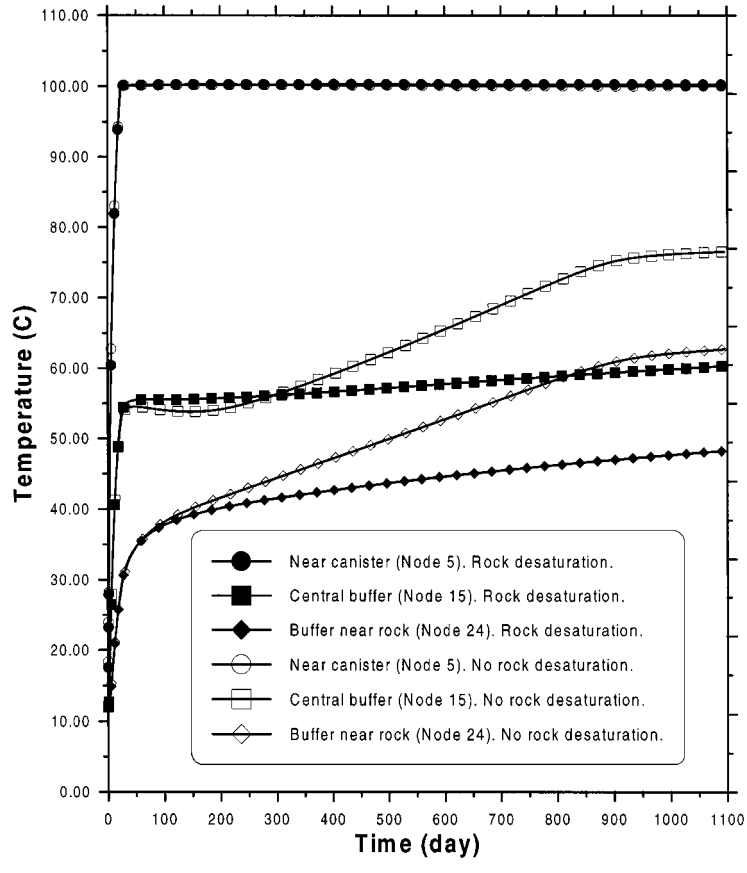

Figure 18. Comparison of temperature variations with time for analyses with and without rock desaturation

retention curves used in the analysis. The existence of two different behaviour zones is nevertheless general.

Computed absolute hydration times will also depend on the prevailing water pressure in the test site. Additional analyses have been carried out adopting an initial water pressure in the granite of 2·5 MPa instead of the reference value of 0·5 MPa. The two alternative granite retention curves used before have been used. As the results of Table II indicate, hydration times are quite sensitive to the granite water pressure. Hydration times are reduced by a factor of 1·5–2·5 when the initial water pressure is increased from 0·5 to 2·5 MPa.

8. CONCLUSIONS

The performance of coupled THM computations in an idealized analysis of a proposed *in situ* test has clearly demonstrated the effects of a number of inter-related phenomena occurring during the

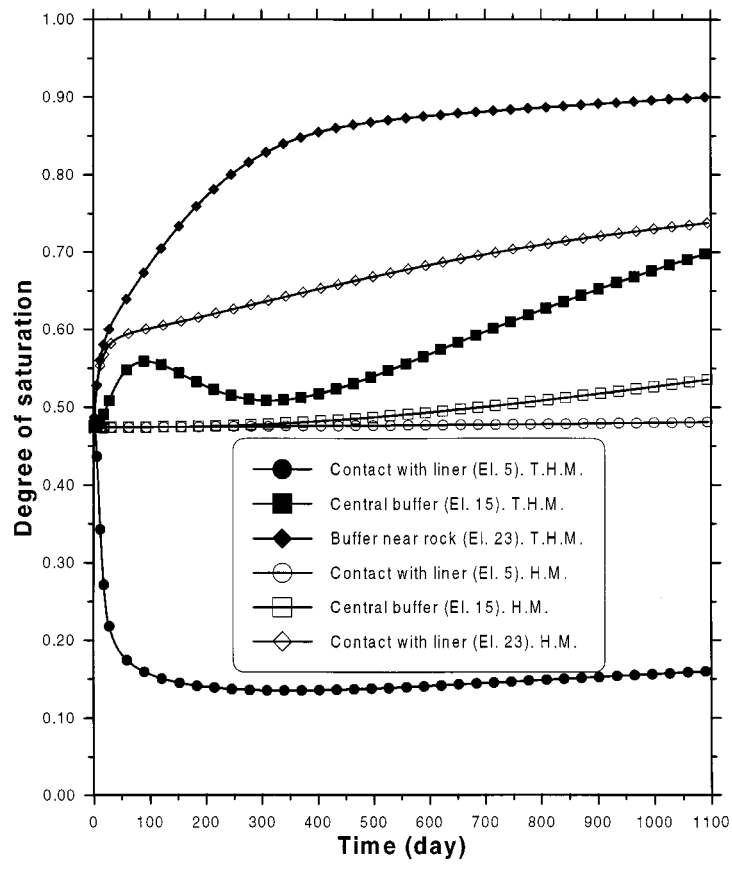

Figure 19. Comparison of the variations of the degree of saturation of HM and THM analyses

simultaneous heating and hydration of an engineered barrier placed in a drift excavated in a granitic rock. It has also been shown that there are a number of features (i.e. vapour diffusion, thermal conductivity variation) that must be included in the analysis to obtain valid results. Unfortunately, the analyses also show that some results can be very sensitive to the variation of the values of parameters that are difficult to measure with precision.

In spite of this, the performance of the series of numerical analyses reported here allows one to draw some conclusions regarding thermal, hydraulic and mechanical aspects of the problem:

Thermal aspects

(1) With the envisaged heating conditions of the *in situ* test, a gradual increase of temperature will occur in the buffer and granite that will extend progressively in the host medium. The buffer temperature reduction during the cooling stage is relatively fast with a quite uniform temperature distribution throughout the engineered barrier.

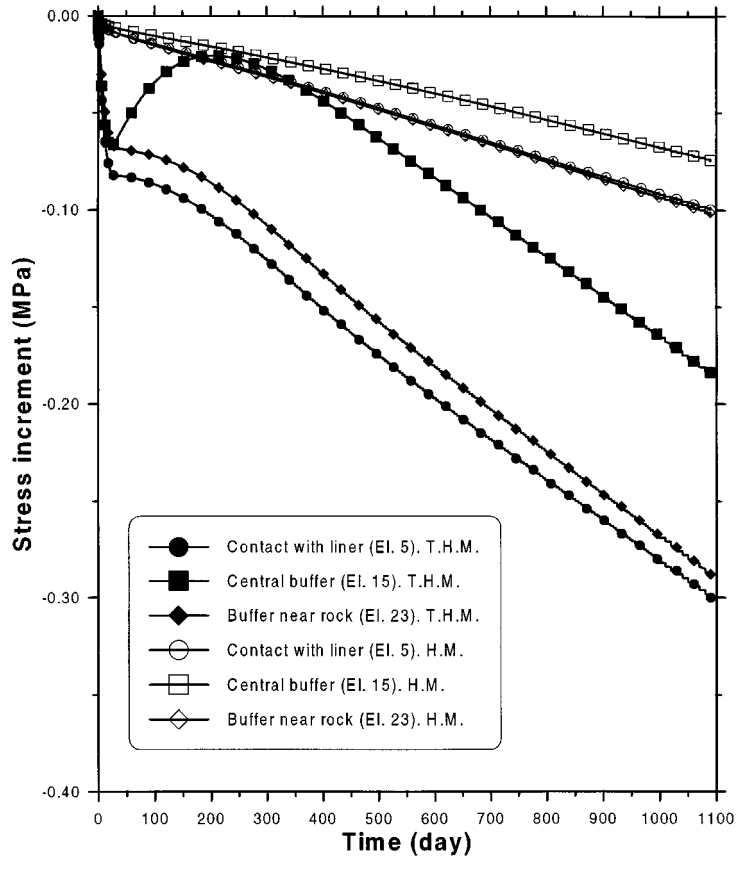

Figure 20. Comparison of the radial stress increment variations for HM and THM analyses

(2) Heat power required to maintain the design maximum temperature in the bentonite may increase with time due to the higher thermal conductivity of the engineered barrier caused by the progressive hydration of the buffer.
(3) The time required to reach the prescribed bentonite maximum temperature is strongly and non-linearly dependent on heating power and the initial value of the thermal conductivity of the buffer.

Hydraulic aspects

(1) With the parameters adopted in the main analysis, the buffer is still far from saturation at the end of the heating stage. The main reason is the hydraulic barrier surrounding the bentonite due to the desaturation of the host rock. Much faster hydration times are obtained in an analysis with an alternative granite retention curve that ensures that no rock desaturation takes place.

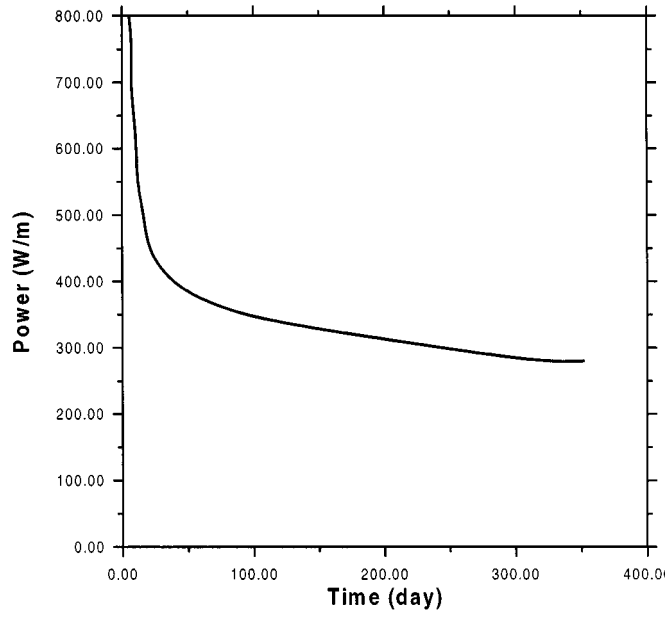

Figure 21. Relationship between heating power and time to reach a temperature of 100°C in the buffer

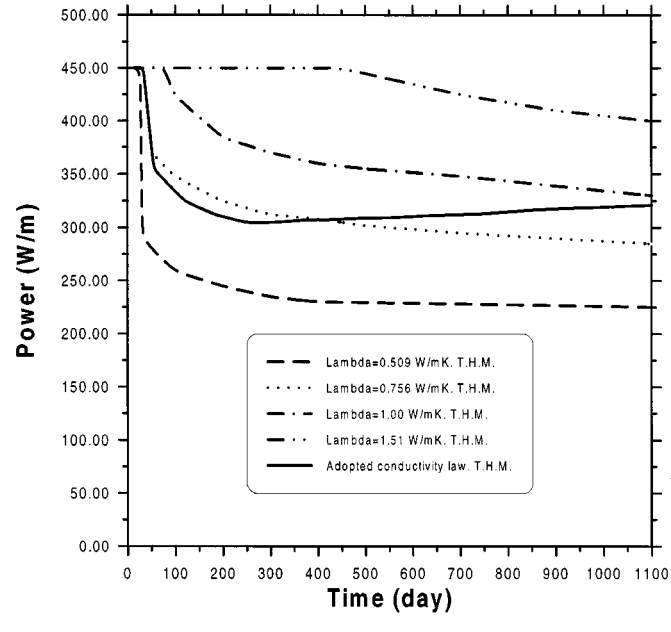

Figure 22. Relationship between heating power and heating time for various values of thermal conductivity and for the THM analysis

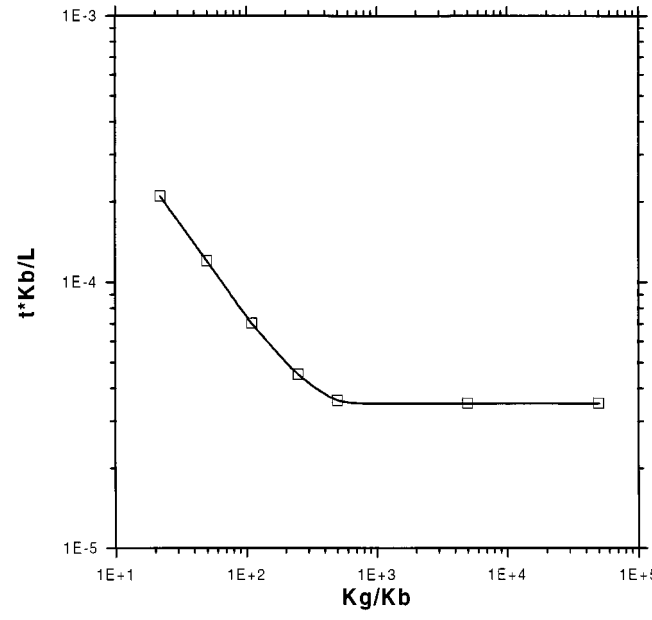

Figure 23. Normalized hydration times as a function of the rock saturated permeability/bentonite saturated permeability ratio ($L = 0{\cdot}66$ m, thickness of the barrier)

Table II. Hydration times for different hydraulic conditions

	Initial granite water pressure 0·5 MPa	Initial granite water pressure 2·5 MPa
Rock desaturation	5375 days	2050 days
No rock desaturation	1625 days	1096 days

(2) Hydration times are naturally controlled by the permeability of granite and bentonite. Performance of a sensitivity analysis permits one to distinguish two zones in which the progress of hydration is controlled by either the permeability of the rock or the permeability of the buffer.
(3) The evolution and progress of hydration is strongly influenced by moisture transfer by vapour diffusion. Increased temperature also assists hydration by decreasing effective permeability.

Mechanical aspects

(1) The low deformability of the granite implies that only small global porosity variations of the engineered barrier take place.
(2) The development of stresses in the buffer is a consequence of a complex interplay between the progressive development of the swelling potential of the bentonite as hydration proceeds and the need to keep overall volume changes to the values provided by the boundary constraints. Because of the complex nature of the stress/strain behaviour of

unsaturated soil, more work is required to examine in more detail the dependence of the mechanical response on the type and parameters of the constitutive law adopted.

ACKNOWLEDGEMENTS

The support of ENRESA in this work is grateful acknowledged. Support has also been provided by the Dirección General de Investigación Científica y Técnica through research grants PB95-0771 and PB93-0964.

NOTATION

$\mathbf{b}$	body force vector in equilibrium equation ($\mathrm{F\,L^{-3}}$)
$\mathbf{D}$	constitutive stiffness matrix ($\mathrm{FL^{-2}}$)
$\mathbf{D}_\alpha^i$	dispersion tensor (i = h, w for α = l and i = w, a for α = g) ($\mathrm{ML^{-1}\,T^{-1}}$)
D_m^w	molecular diffusion coefficient ($\mathrm{L^2\,T^{-1}}$)
$\mathbf{D}_\mathrm{g}'$	mechanical dispersion tensor ($\mathrm{L^2\,T^{-1}}$)
E_α	internal energy of α-phase per unit mass of α-phase ($\mathrm{EM^{-1}}$)
E_α^i	internal energy of i-species in α-phase per unit mass of i-species ($\mathrm{EM^{-1}}$
f^i	external mass supply per unit volume of medium (i = h, w, a) ($\mathrm{ML^{-3}\,T^{-1}}$)
f^E	internal/external energy supply per unit volume of medium ($\mathrm{EL^{-3}\,T^{-1}}$)
G	elastic shear modulus ($\mathrm{FL^{-2}}$)
$\mathbf{g}$	gravity vector ($\mathrm{LT^{-2}}$)
$\mathbf{h}$	constitutive vector for suction effects ($\mathrm{FL^{-2}}$)
i	species index, w water and a air (superscript)
$\mathbf{I}$	identity matrix (dimensionless)
$\mathbf{i}_\alpha^i$	non-advective mass flux ($\mathrm{ML^{-2}\,T^{-1}}$)
$\mathbf{i}_\mathrm{c}$	nonadvective heat flux ($\mathrm{EL^{-2}\,T^{-1}}$)
$\mathbf{j}_{\mathrm{E}\alpha}$	advective energy flux in α-phase w.r.t. a fixed reference system ($\mathrm{EL^{-2}\,T^{-1}}$)
$\mathbf{j}_\alpha^i$	total mass flux of i-species in α-phase w.r.t. a fixed reference system ($\mathrm{ML^{-2}\,T^{-1}}$)
K	elastic bulk modulus ($\mathrm{FL^{-2}}$)
$\mathbf{K}_\alpha$	permeability tensor (α = l, g) ($\mathrm{M^{-1}\,L^3\,T}$)
$\mathbf{k}$	intrinsic permeability tensor ($\mathrm{L^2}$)
$k_{\mathrm{r}\alpha}$	α-phase relative permeability (α = l, g) (dimensionless)
M_a	molecular mass of air (M) (0·02895 $\mathrm{kg\,mol^{-1}}$)
M_w	molecular mass of water (M) (0·018 $\mathrm{kg\,mol^{-1}}$)
$\mathbf{m}$	auxiliary vector dimensionless
P_α	fluid pressure of α-phase (α = l, g) ($\mathrm{FL^{-2}}$)
P_a	partial pressure of air ($\mathrm{FL^{-2}}$)
$\mathbf{q}_\alpha$	volumetric flux of α-phase w.r.t. the solid matrix (α = l, g) ($\mathrm{LT^{-1}}$)
R	constant of gases ($\mathrm{E\Theta^{-1}}$) (8·314 $\mathrm{J\,mol^{-1}\,K^{-1}}$)
S_α	volumetric fraction of pore volume occupied by α-phase (α = l, g) (dimensionless)
S_e	$[(s_\mathrm{l} - S_\mathrm{lr})/(S_\mathrm{ls} - S_\mathrm{lr})]$ effective liquid saturation (dimensionless)
S_lr	residual liquid saturation (dimensionless)
S_ls	maximum liquid saturation (dimensionless)
T	temperature (Θ)
$\mathbf{u}$	solid displacement vector (L)

α	phase index, s solid, l liquid and g gas (subscript)
$\boldsymbol{\varepsilon}$	strain tensor (dimensionless)
ε_v	volumetric strain (dimensionless)
θ^i_α	$(= \omega^i_\alpha \rho_\alpha)$ mass of *i*-species per unit volume of α-phase (ML^{-3})
λ	thermal conductivity $(E\Theta^{-1}L^{-1}T^{-1})$
λ_α	α-phase thermal conductivity $(E\Theta^{-1}L^{-1}T^{-1})$
λ_{dry}	thermal conductivity for dry state $(E\Theta^{-1}L^{-1}T^{-1})$
λ_{sat}	thermal conductivity for saturated state $(E\Theta^{-1}L^{-1}T^{-1})$
μ_α	dynamic viscosity of α-phase $(\alpha = l, g)$ $(FL^{-2}T)$
$\mathbf{\nabla}$	gradient vector (L^{-1})
ρ_α	mass of α-phase per unit volume of α-phase (ML^{-3})
ϕ	porosity (dimensionless)
$\boldsymbol{\sigma}$	stress tensor (FL^{-1})
$\boldsymbol{\sigma}'$	effective stress tensor (FL^{-2})
τ	tortuosity (dimensionless)
ω^i_α	mass fraction of *i*-species in α-phase (dimensionless)

For simplicity F (force), M (mass), L (length), T (time), E (energy) and Θ (temperature) are used as primary quantities.

REFERENCES

1. S. Olivella, J. Carrera, A. Gens and E. E. Alonso, 'Non-isothermal multiphase flow of brine and gas thorough saline media', *Transport in Porous Media*, **15,** 271–293 (1994).
2. D. Gawin, P. Baggio and B. A. Schrefler, 'Coupled heat, water and gas flow in deformable porous media', *Int. J. Numer. Meth. Fluids*, **20,** 969–987 (1995).
3. H. R. Thomas and Y. He, 'An analysis of coupled heat, moisture and air transfer in a deformable unsaturated soil', *Géotechnique*, **45,** 677–689 (1995).
4. H. R. Keusen, J. Ganguin, P. Schuler, M. Buletti, *Grimsel Test Site. Geology*, Technical Report 87-14E, Nagra, Baden, Switzerland, 1989.
5. S. Panday and M. Y. Corapcioglu, 'Reservoir transport equations by compositional approach', *Transport in Porous Media* **4,** 369–393 (1989).
6. M. T. Sprackling, in: *Liquids and Solids*, Student Physics Series, King's College, University of London. Routledge and Kegan Paul, (eds.) 1985.
7. N. E. Edlefson and A. B. C. Anderson, 'Thermodynamics of soil moisture', *Hilgardia*, **15**(2)**,** 31–298 (1943).
8. M. A. Lovell, 'Thermal conductivities of marine sediments', *Q. J. Engng. Geology*, **18,** 437–441 (1985).
9. R. van Genuchten, 'A closed-from equation for predicting the hydraulic conductivity of unsaturated soils', *Soil Sci. Soc. Am. J*., **49,** 892–898 (1980).
10. D. W. Pollock, 'Aimulation of fluid flow and energy transport processes associated with high-level radioactive waste disposal in unsaturated alluvium', *Water Resources Res.* **22**(5)**,** 765–775 (1986).
11. A. Lloret and E. E. Alonso, 'State surfaces for partially saturated soils', *Proc. 11th ICSMFE*, San Francisco, Vol. 2, 1985, 557–562.
13. E. E. Alonso, A. Gens and A. Josa, 'A constitutive model for partially saturated soils', *Géotechnique*, **40,** 405–430 (1990).
14. A. Gens and E. E. Alonso, 'A framework for the behaviour of unsaturated expansive clays', *Can. Geotech. J*. **29,** 1013–1032 (1992).
15. A. Gens, 'Constitutive laws', in: *Modern Issues in Non-saturated Soils*, Springer, Wien, 1995, pp. 129–158.
16. S. Olivella, A. Gens, J. Carrera and E. E. Alonso, 'Numerical formulation for a similar (CODE-BRIGHT) for the coupled analysis of saline media', *Engng. Comput*., **13,** 87–112 (1996).
17. M. V. Villar, 'Modelling and validation of the thermal-hydraulic-mechanical and geochemical behaviour of the clay barrier. *Final Report 1991–1994*', CIEMAT, Madrid, 1994.
18. B. Frieg and S. Vomvoris, 'Investigation of hydraulic parameters in the saturated and unsaturated zone of the ventilatin drift,' *Technical Report 93-10*, Nagra, Baden, Switzerland, 1994.
19. H. R. Thomas, Y. He, A. Ramesh, Z. Zhou and M. V. Villar, J. Cuevas, 'Heating unsaturated clay—An experimental and numerical investigation', *Proc. 3rd. Eur. Conf. Numerical Meth. in Geomech.* Manchester, 1994, pp. 181–186.

